The Electron–Hole Bilayer TFET: Dimensionality Effects and Optimization

(Article begins on next page)

19 February 2025

The Electron-Hole Bilayer TFET: Dimensionality Effects and Optimization

Cem Alper, *Student Member, IEEE,* Pierpaolo Palestri, *Senior Member, IEEE,* Jose Luis Padilla and Adrian M. Ionescu, *Senior Member, IEEE*

Abstract

An extensive parameter analysis is performed on the Electron-Hole Bilayer Tunnel FET (EHBTFET) using a 1D effective mass (EMA-NP) Schrödinger/Poisson solver with non-parabolic corrections considering thin InAs, $In_{0.53}Ga_{0.47}As$, Ge, $Si_{0.5}Ge_{0.5}$ and Si films. It is found that depending on the channel material and channel thickness, the EHBTFET can operate either as a 2D-2D or 3D-3D tunneling device. InAs offers the highest I_{ON}, whereas for Si and $Si_{0.5}Ge_{0.5}$ EHBTFET significant current levels cannot be achieved within a reasonable voltage range. The general trends are explained through an analytical model which shows a close agreement with numerical results.

Index Terms

Band-to-band tunneling, Tunnel Field-Effect Transistor (TFET), EHBTFET, density of states, 2D-2D tunneling, quantum mechanical simulation.

I. Introduction

The research on tunnel field effect transistors (TFET) has picked up considerable pace recently [1], mainly due to its demonstrated potential [2] to overcome the thermionic emission barrier that makes it a suitable candidate as a 'steep slope switch' [3]. Since TFETs make use of the quantum mechanical band-to-band tunneling (BTBT) and typically thin film structures are utilized, it is imperative to use adequate tools that inherently take into account the size-induced quantization effects. Such effects, in most cases, alter the dimensionality of the carrier gas involved in the tunneling process and therefore, can potentially change the device characteristics.

Among many different TFET architectures, the electron-hole bilayer TFET (EHBTFET) [4] stands out as a particularly attractive option as it exploits the step-like density of states (DOS) in 2D quantized layers [5]. Although it was simulated using different approaches and several issues concerning the engineering of such a structure have been investigated in recent papers [6], [7], an extensive parameter analysis to estimate the order of magnitude of the ON current (I_{ON}) and the main parameters affecting I_{ON} is yet to be done. This paper presents a detailed investigation of the parameter space of the EHBTFET through a computationally efficient effective-mass Schrödinger-Poisson solver with non-parabolicity corrections (EMA-NP). The general trends are explained through an analytical model.

The paper is organized as follows: Section II briefly describes the numerical model for direct and phonon-assisted BTBT. Section III introduces the device structure and the material parameters space used in the numerical simulations. Section IV presents the simulation results and discusses the impact of the dimensionality of the carrier gases involved in the tunneling process. This latter section also presents an analytical model to further help explaining the results. Section V summarizes the main findings.

II. Numerical Model Description & General Framework

The simulator solves the Schrödinger and Poisson equations self-consistently under the effective mass approximation with non-parabolicity corrections [8]. Self-consistency is achieved using the non-linear Schrodinger-Poisson scheme [9]. The electrons and holes are assumed to be in equilibrium with the drain and source terminals respectively, hence $E_{Fn} = -qV_D$ and $E_{Fp} = -qV_S$. The influence of non-parabolicity on the density of states (DOS) and on the wavefunctions is taken into account following Troger *et al.* [10]. The non-diagonal effective mass tensor of the Ge equi-energy ellipsoids is mapped to a diagonal tensor following the procedure given by Rahman *et al.* [11]. Once self-consistency is achieved, the BTBT rate is estimated using corresponding models for the phonon-assisted and direct BTBT [5].

The expression for direct BTBT between the valence band and the conduction band minima at the Γ point is given by [8], which sums up the contributions of all aligned electron and hole subband pairs:

TABLE I
BANDGAPS, EFFECTIVE MASSES (ALONG THE QUANTIZATION AND TRANSVERSE DIRECTIONS), VALLEY DEGENERACIES, NONPARABOLICITY COEFFICIENTS ALONG WITH DEFORMATION POTENTIALS AND PHONON ENERGIES (PHONON-ASSISTED BTBT ONLY) USED FOR NUMERICAL SIMULATIONS.

Material (Valley)	$E_G[\mathrm{eV}]$	$m_{e,q}^*[\mathrm{m_0}]$	$m_{e,\perp}^*[\mathrm{m_0}]$	$m_{hh}^*[\mathrm{m_0}]$	$m_{lh}^*[\mathrm{m_0}]$	$\alpha[\mathrm{eV^{-1}}]$	$D[\mathrm{eV/m}]$	$E_{ph}[\mathrm{meV}]$
Si (Δ_4)	1.12	0.1905	0.417	0.49	0.16	0.5	8.16×10^{10}	18.6
Si (Δ_2)		0.916	0.1905					
Si$_{0.5}$Ge$_{0.5}$ (Δ_4)	0.91	0.1905	0.417	0.41	0.102	0.5	7.98×10^{10}	13.6
Si$_{0.5}$Ge$_{0.5}$ (Δ_2)		0.916	0.1905					
Ge (L_4)	0.66	0.117	0.292	0.33	0.043	0.33	7.8×10^{10}	6
Ge (Γ)	0.8	0.043	0.043			0.85	-	-
InAs	0.358	0.022	0.022	0.41	0.025	3.6	-	-
In$_{0.53}$Ga$_{0.47}$As	0.751	0.042	0.042	0.457	0.052	1.5	-	-

$$I_{dir} = \frac{4\pi q W L_G}{\hbar} \sum_{k} \sum_{\alpha'=\{HH,LH\},k'} |M_{dir}|^2 \times \tag{1}$$
$$JDOS(E_T)\Theta(E_{k'\alpha'} - E_{k\Gamma})(f_c(E_T) - f_v(E_T))$$

where $E_{k'\alpha'}$, $E_{k\Gamma}$ are the quantized energies for the hole and electron states, respectively. k' and k are the subband indices for hole and electron states. The index α' runs over the heavy holes (HH) and light holes (LH). L_G and W are respectively the gate length and device width (which extends along the y-direction). The $JDOS(E_T)$ is the joint density of states for each aligned electron-hole subband pair that conserves both the total energy (E_T) and the transverse momentum [12]. $f_{c,v}$ are the Fermi-Dirac distributions of the conduction and valence bands, respectively. M_{dir} is the coupling element between the electron and hole states and calculated using a model based on Kane's two band dispersion [13], given as:

$$M_{\mathrm{dir}} = q\sqrt{\frac{\hbar^2}{4\overline{m}E_G^\Gamma}}C_0(\theta)\delta_{k_\perp,k'_\perp}\int \psi_{k\Gamma}^*(z)|F(z)|\psi_{k'\alpha'}(z)dz \tag{2}$$

where $\overline{m} = \frac{2m_e^* m_h^*}{m_e^* + m_h^*}$, $F(z)$ is the electric field and $C_0(\theta)$ is the form factor caused by the polarization dependence of the matrix elements [5], [14], [15]. This dependence stems from the symmetry properties of HH and LH basis vectors and from the fact that the k-space is limited along the quantization direction compared to the bulk case. The averaging of the coupling matrix element is thus done in two dimensions (i.e. on a circle) instead of three dimensions as in bulk semiconductors. This introduces a dependence of the magnitude of the coupling matrix element on the wave-vector direction, denoted as $C_0(\theta)$[14].

The phonon-assisted BTBT current is calculated following [16]:

$$I_{ph} = \frac{2qL_G W}{\hbar}\int \frac{dE}{2\pi} \cdot (\{f_v(E)[1 - f_c(E - \hbar\omega_{k_0})][\nu(\hbar\omega_{k_0}) + 1]$$
$$- f_c(E - \hbar\omega_{k_0})[1 - f_v(E)]\nu(\hbar\omega_{k_0})\}T_v^{em}(E)$$
$$+ \{f_v(E)[1 - f_c(E + \hbar\omega_{k_0})]\nu(\hbar\omega_{k_0})$$
$$- f_c(E + \hbar\omega_{k_0})[1 - f_v(E)][\nu(\hbar\omega_{k_0}) + 1]\}T_v^{abs}(E)) \tag{3}$$

where $\nu(\hbar\omega_{k_0})$ is the Bose-Einstein distribution for the phonon with energy $E_{ph} = \hbar\omega_{k_0}$ connecting the valence band and conduction band extrema. $T_v^{em,abs}(E)$ are the transmission coefficients that are based on the spectral functions, which contain the information about the wavefunctions and the density of states. We refer the reader to [8], [12], [16] for the exact expressions of $T_v^{em,abs}(E)$ and of the spectral functions, which are omitted here for brevity.

It is worth noting that for both direct and phonon-assisted BTBT, the tunneling current is determined by three components: i) the coupling element $M_{dir(ph)}$, ii) the density of states (J)DOS and iii) the Fermi occupation term.

The anti-crossing between LH and HH branches [17] has been included to account for the drastic asymmetry of the effective masses of the real and imaginary branches of the hole subbands and the light hole mass was used as the effective mass of the heavy hole imaginary branch for direct BTBT [18]. Effectively, this results in quantized energy levels mostly being determined by the effective mass of the heavy holes, whereas the tunneling probability is determined by the light hole mass.

The direct BTBT model has been validated against k · p and tight-binding models elsewhere considering InAs and Ge diodes with different doping levels [8]. Fig. 1 shows, as a further verification, that our model for direct tunneling in Ge, without any adjustment, reproduces the experimental data for Ge diodes collected in [19]. The deformation potential and the phonon energy parameters for Ge are taken from [20]. The parameters for phonon-assisted tunneling (for Si) have been calibrated against experimental data [19], [21] (see Fig. 1). The deformation potential for Si$_{0.5}$Ge$_{0.5}$ was linearly interpolated from the Si and Ge values. Phenomena such as trap-assisted tunneling [22] and band tails in the energy gap [6], that may have a significant impact on the experimental TFET devices are not included at present in the simulations.

Note that, although BTBT in bulk Ge is dominated by direct transitions (since the conduction band minimum is only 0.14eV higher than the actual bandgap), the situation is much different under strong quantization, since the low mass of the Γ valley results in a much larger gap for direct transitions, so that phonon assisted BTBT would dominate.
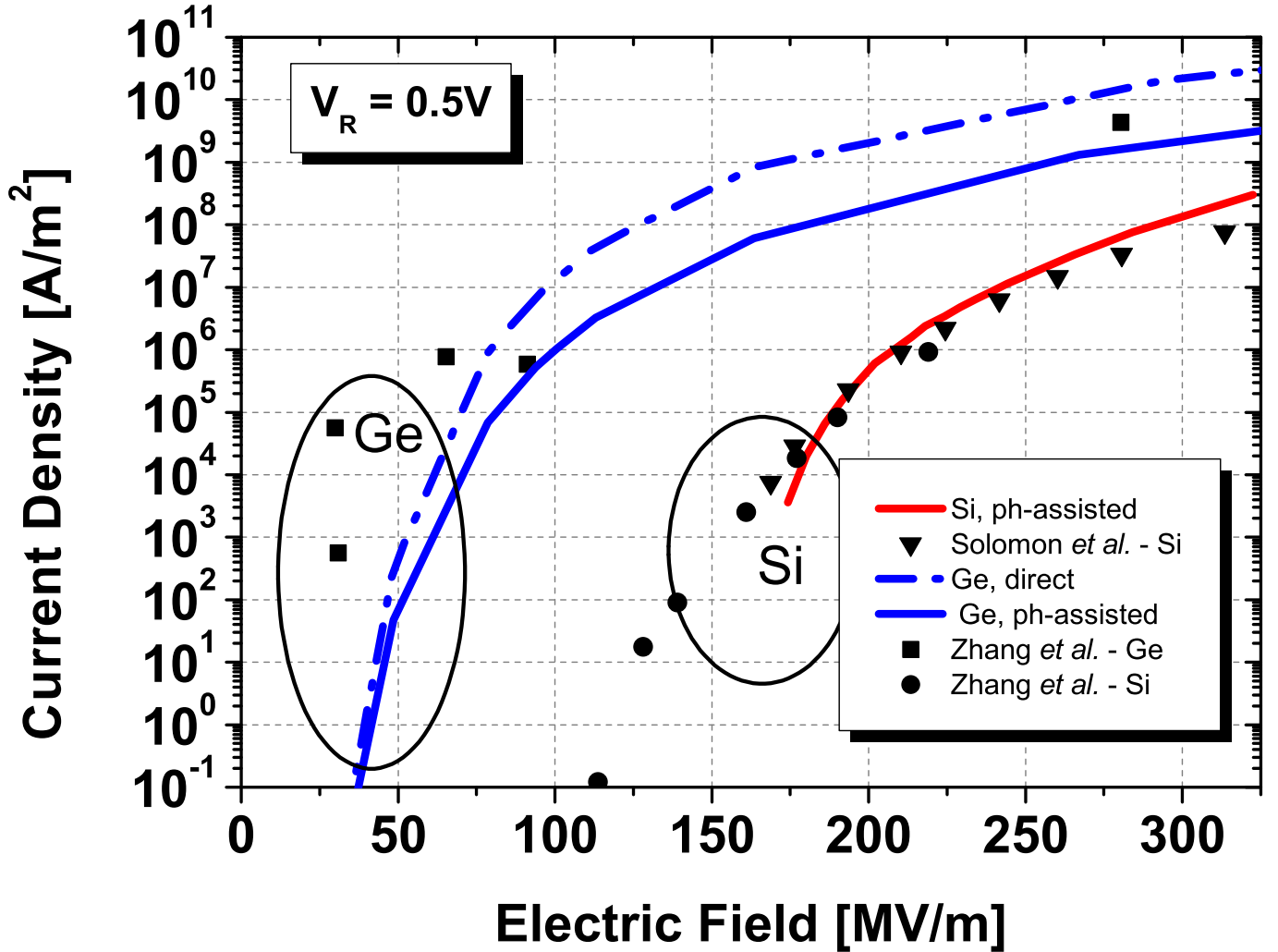

Fig. 1. Current versus maximum electric field for experimentally measured [19], [21] (symbols) and simulated (lines) tunnel diodes under a reverse bias of 0.5V.

III. DEVICE STRUCTURE & PARAMETER SPACE

The EHBTFET consists of a thin semiconductor layer sandwiched in between two gates biased with opposite polarities (see Fig. 2). This allows for the formation of the 2D electron and hole gases (2DEG and 2DHG, respectively) which are quantized into subbands. Once the subband energies of the electrons (E_{e}) and holes (E_{h}) are aligned, BTBT takes place between the two layers.

For the simulations, we take a 1D vertical slice in the overlap region and assume translational symmetry along the x-direction (i.e. horizontal potential profile constant in the overlap region). This assumption relies on the fact that the vertical potential profile in the overlap region is very close in both 1-D and 2-D simulations [5]. Since we are using a 1D model, the switching is considered as 'ideal', i.e. no predictions about the OFF current and the corresponding point switching slope can be done. That being said, we note that lateral effects can be suppressed very efficiently using hetero-gate configurations [23] or underlap counterdoping [24].

We perform anti-symmetric gate sweeps (i.e. sweep the n and p gates simultaneously with $V_{\mathrm{n-gate}} = -V_{\mathrm{p-gate}}$), since it was shown to have lower lateral leakage and better subthreshold slopes [5]. Midgap gate workfunctions have been considered. Different channel materials (Si, Si$_{0.5}$Ge$_{0.5}$, Ge, InAs and In$_{0.53}$Ga$_{0.5}$As), film thicknesses ($T_{\mathrm{CH}} = [7.5, 20]$nm) and oxide thicknesses ($T_{\mathrm{OX}} = [0.5, 3]$nm) are employed. In terms of the channel material, we limit ourselves to homojunction architectures, although significant improvement can be obtained by utilizing staggered and broken gap III-V heterostructures [25], [26].
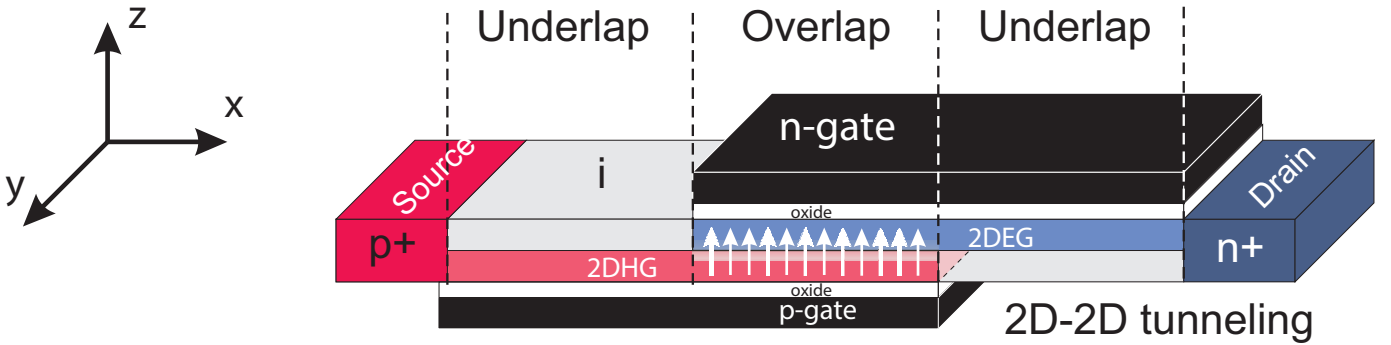
Fig. 2. The EHBTFET device structure. $L_{\mathrm{OVERLAP}} = 50\mathrm{nm}$, $V_{\mathrm{DS}} = 0.15\mathrm{V}$ for all simulations. $\epsilon_{\mathrm{oxide}} = 3.9\epsilon_0$.

The device is assumed to be oriented along the [100] direction. For Si, six Δ valleys (four-fold degenerate Δ_4 with transverse mass along the z direction and two-fold degenerate Δ_2 with longitudinal mass along the z direction) have been taken into account. Since we are using a mole fraction of 0.5 for SiGe, the effective masses for the Δ valleys are taken the same as in Si [27]. For Ge, four-fold degenerate L valleys and the direct gap Γ valley have been considered, so both phonon-assisted and direct BTBT are included. For InAs and $\mathrm{In}_{0.53}\mathrm{Ga}_{0.47}\mathrm{As}$, only the conduction band valley in Γ is included since the other valleys sit far apart energetically. The material parameters used in the simulations and calculations are listed in Table I.

IV. RESULTS & DISCUSSION

A. Impact of Carrier Dimensionality

The left plots in Fig. 3 depict the alignment voltage (defined as $V_{\mathrm{align}} = V_{\mathrm{n-gate}} - V_{\mathrm{p-gate}} = 2V_{\mathrm{n-gate}}$) for which the lowest electron and the highest hole subband get aligned, whereas the right plots report the I_{ON} (defined as I_{D} at $V_{\mathrm{n-gate}} = \frac{V_{\mathrm{align}}}{2} + V_{\mathrm{DS}} = -V_{\mathrm{p-gate}}$ with $V_{\mathrm{DS}} = 0.15\mathrm{V}$). Si, $\mathrm{Si}_{0.5}\mathrm{Ge}_{0.5}$ and Ge results are dominated by phonon-assisted BTBT. Although direct BTBT is included in Ge, it is found not to dominate the current in Ge EHBTFETs for the considered bias, contrarily to what happens in the bulk diodes of Fig. 1 since the quantized energies of the Γ electrons are much higher than those of L valleys. For InAs and $\mathrm{In}_{0.53}\mathrm{Ga}_{0.47}\mathrm{As}$ EHBTFETs only direct BTBT takes place. Comparing the Ge, $\mathrm{In}_{0.53}\mathrm{Ga}_{0.47}\mathrm{As}$ and InAs results, it is seen that the overall behavior with respect to parameter changes is similar, except for the drastically higher I_{ON} of the InAs EHBTFET due to small direct bandgap.

A close inspection on the I-V characteristics of Ge, InAs and $\mathrm{In}_{0.53}\mathrm{Ga}_{0.47}\mathrm{As}$ EHBTFETs reveals that vertical contour lines in the ON current plots are caused by the fact that 2D-2D tunneling takes place in those cases. In this context 2D-2D tunneling means that only one electron-hole subband pair gets aligned to contribute to the BTBT current.

The behavior of I_{ON} with respect to the parameters drastically changes for Si EHBTFET (Fig. 3 top right) with thicker channel thicknesses ($T_{\mathrm{CH}} > 12.5\mathrm{nm}$). In those cases, the high effective masses of Si Δ_2 valleys and heavy holes allow for the formation of a quasi-3D continuum of states (i.e. many subband pairs get aligned, see Fig. 4). This is due to the fact that heavier mass reduces the energy spacing between quantized levels, resulting in (pseudo) 3D-3D tunneling. A similar comment can be made for $\mathrm{Si}_{0.5}\mathrm{Ge}_{0.5}$ EHBTFET as well, due to the similar effective mass values, even though the alignment voltage is relatively smaller due to reduced bandgap. For both Si and SiGe, an interesting feature of the contour plots is that as the channel thickness is reduced from the relatively large values (20nm), a *decrease* in the ON current is seen. This is actually caused by the reduction of the DOS available for tunneling, which is stronger than the competing increase in the tunneling rate brought in by the thinner channel. Eventually, as the channel is further thinned down, the tunneling rate increase starts to counterbalance the effects related to the DOS reduction and the current is enhanced.

This drastic difference between 2D-2D tunneling (Ge and III-Vs in Fig. 3) and 3D-3D tunneling (Si and $\mathrm{Si}_{0.5}\mathrm{Ge}_{0.5}$ in Fig. 3) clearly demonstrates that the carrier gas dimensionality plays an important role in determining the influence of device parameters on the drive current. *A limit on the obtainable current is imposed for 2D-2D tunneling due to the reduction of the available states for tunneling, independently of the electrostatic control of the channel.* This is in stark contrast to 3D-3D tunneling, where a better electrostatic control would always yield higher ON current for the same bias.

This latter point is better visualized by the I-V characteristics given for a 2D-2D tunneling device (i.e. a Ge EHBTFET with $T_{\mathrm{CH}} = 7.5\mathrm{nm}$) versus a pseudo 3D-3D tunneling one (i.e. a Si EHBTFET with $T_{\mathrm{CH}} = 15\mathrm{nm}$) in Fig. 5. It is seen that in 3D-3D tunneling a thinner oxide increases the ON current as well as shifting the onset of tunneling to lower gate biases, whereas only a rigid shift of the tunneling onset is seen for 2D-2D tunneling.

Another distinguishing feature between the 2D-2D and 3D-3D tunneling is that the I-V characteristics for the former generally exhibit a negative transconductance behavior [12] as seen in Fig. 5, which stems from the wavefunction repulsion as the electric field increases and from the step-like 2D DOS which does not change with the gate bias. This is also observed in Fig. 3 for
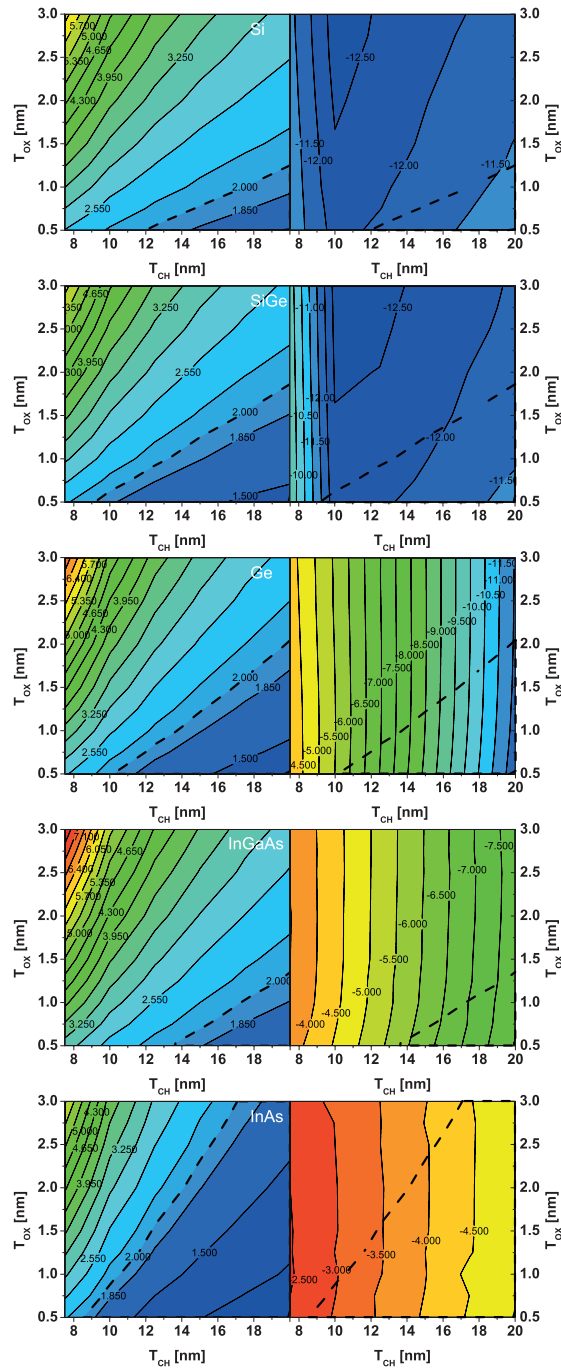
Fig. 3. Contour plots of (Left) The alignment voltage V_{align}, (Right) The $\log_{10} I_{\text{ON}}[\text{A}/\mu\text{m}]$ for (top to bottom) Si, Si$_{0.5}$Ge$_{0.5}$, Ge, In$_{0.53}$Ga$_{0.47}$As and InAs EHBTFETs. The dashed contour line corresponds to $V_{\text{align}} = 2\text{V}$. $V_{\text{DS}} = 0.15\text{V}$. I_{ON} is defined as I_{D} at $V_{\text{n-gate}} = \frac{V_{\text{align}}}{2} + V_{\text{DS}} = -V_{\text{p-gate}}$. The differences in the contour profile of the $\log_{10} I_{\text{ON}}$ plots for Si and Si$_{0.5}$Ge$_{0.5}$ w.r.t. Ge and III-Vs are due to the peculiar features of 2D-2D and 3D-3D tunneling mechanisms.

the 2D-2D tunneling cases, which show a slight decrease in ON current for the same T_{CH} as T_{OX} is decreased. Wavefunction repulsion also occurs for 3D-3D tunneling, but the effect is screened by the addition of new states for tunneling as the gate bias increases. Similarly, the decrease of T_{OX} for a given T_{CH} results in an increase in ON current for the same reason, in contrast to the 2D-2D tunneling case.

B. Analytical Model

To better explain the results of the numerical model and investigate the characteristic features of 2D-2D tunneling, an analytical model has been derived by solving the 1D vertical Poisson equation in the overlap region under the depletion
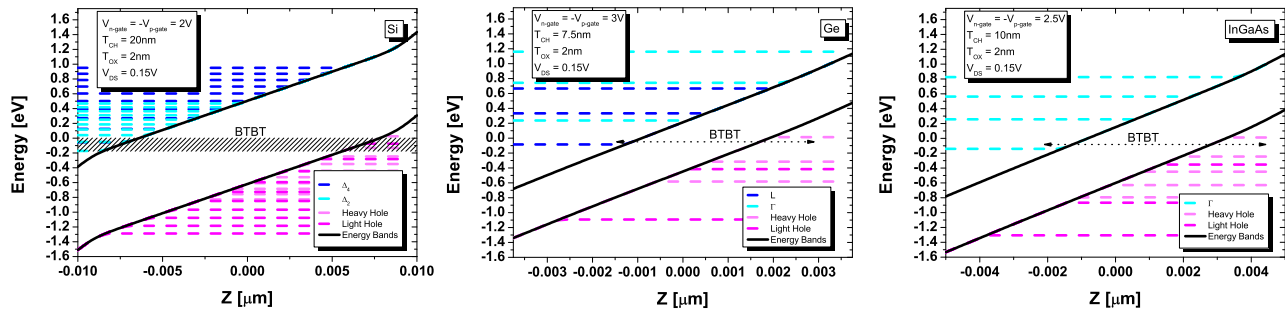
Fig. 4. Energy bands and quantized subband energies (dashed lines) for (Left) Si EHBTFET with $T_{CH} = 20$nm (Middle) Ge EHBTFET with $T_{CH} = 7.5$nm (right) InGaAs EHBTFET with $T_{CH} = 10$nm. Si EHBTFET exhibits 3D-3D tunneling behavior since multiple subbands get aligned, whereas for Ge and InGaAs EHBTFETs only one subband pair is aligned, hence resulting in 2D-2D tunneling behavior.
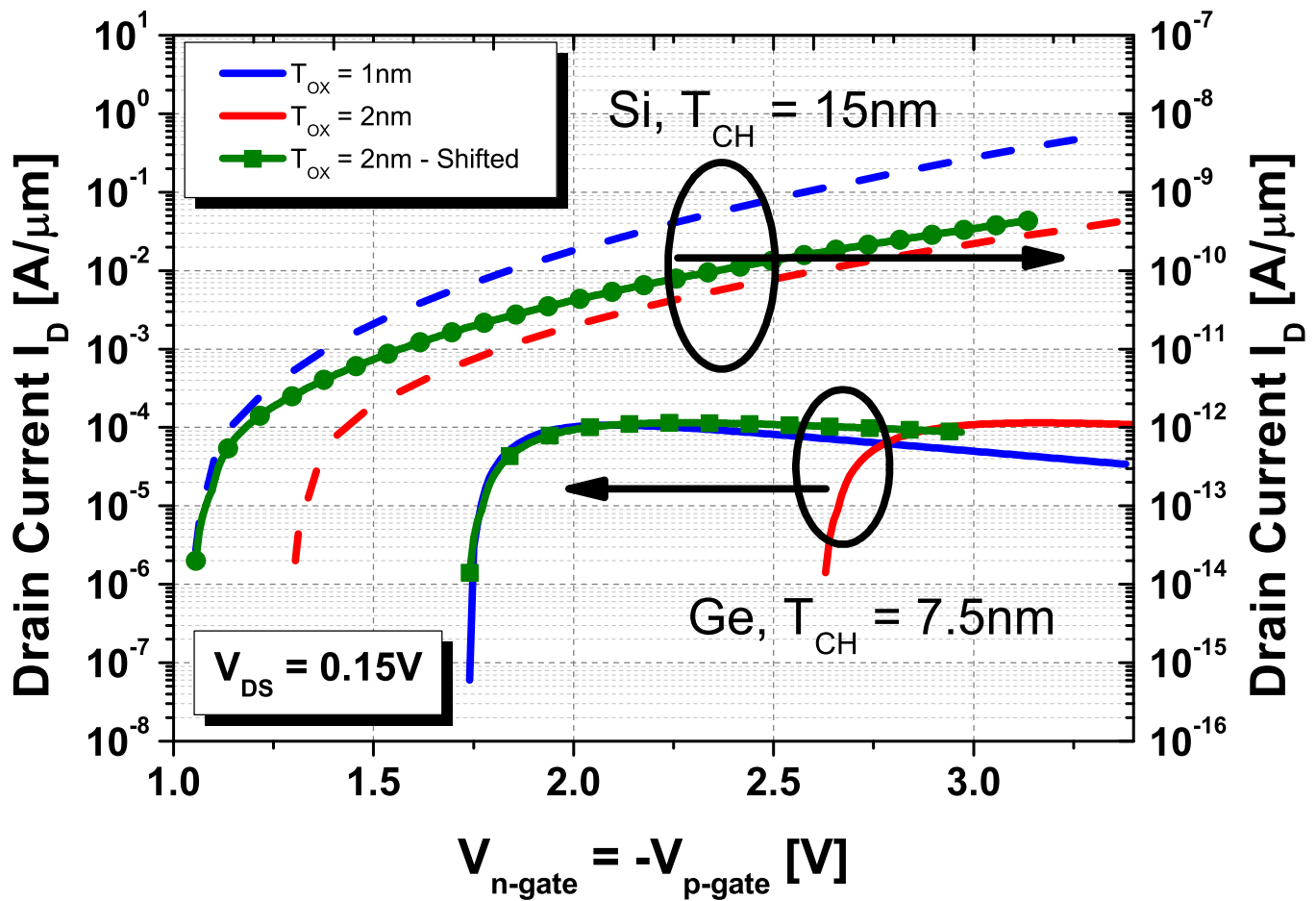

Fig. 5. I-V transfer characteristics for (Left y-axis) Ge EHBTFETs with $T_{CH} = 7.5$nm (2D-2D tunneling) and (Right y-axis) Si EHBTFETs with $T_{CH} = 15$nm (3D-3D tunneling). (blue) $T_{OX} = 1$nm (red) $T_{OX} = 2$nm. $V_{DS} = 0.15$V. The green curves are the artificially shifted versions of the $T_{OX} = 2$nm cases to align at the same onset voltage of the $T_{OX} = 1$nm devices. Note the different scales of the left and right y-axes.

approximation [28]. Neglecting the fixed dopant charges, since a very light doping $N_A = 10^{15}$cm^{-3} is used, the electrostatic potential inside the device is given by:

$$V(z) = -Fz + \frac{V_{p-gate} + V_{n-gate}(1 + \frac{C_{OX}}{C_{CH}})}{2 + \frac{C_{OX}}{C_{CH}}}$$

(4)

$$F = \frac{C_{\mathrm{OX}}}{\epsilon_{\mathrm{CH}}} \left(\frac{V_{\mathrm{n-gate}} - V_{\mathrm{p-gate}}}{2 + \frac{C_{\mathrm{OX}}}{C_{\mathrm{CH}}}} \right) \tag{5}$$

The capacitances per unit area are defined as $C_{\mathrm{CH,(OX)}} = \frac{\epsilon_{\mathrm{CH,(OX)}}}{T_{\mathrm{CH,(OX)}}}$. Fig. 6(a) compares the analytical potential profiles against numerical results: they perfectly match when no inversion charge is induced and a good overall match is observed in general.
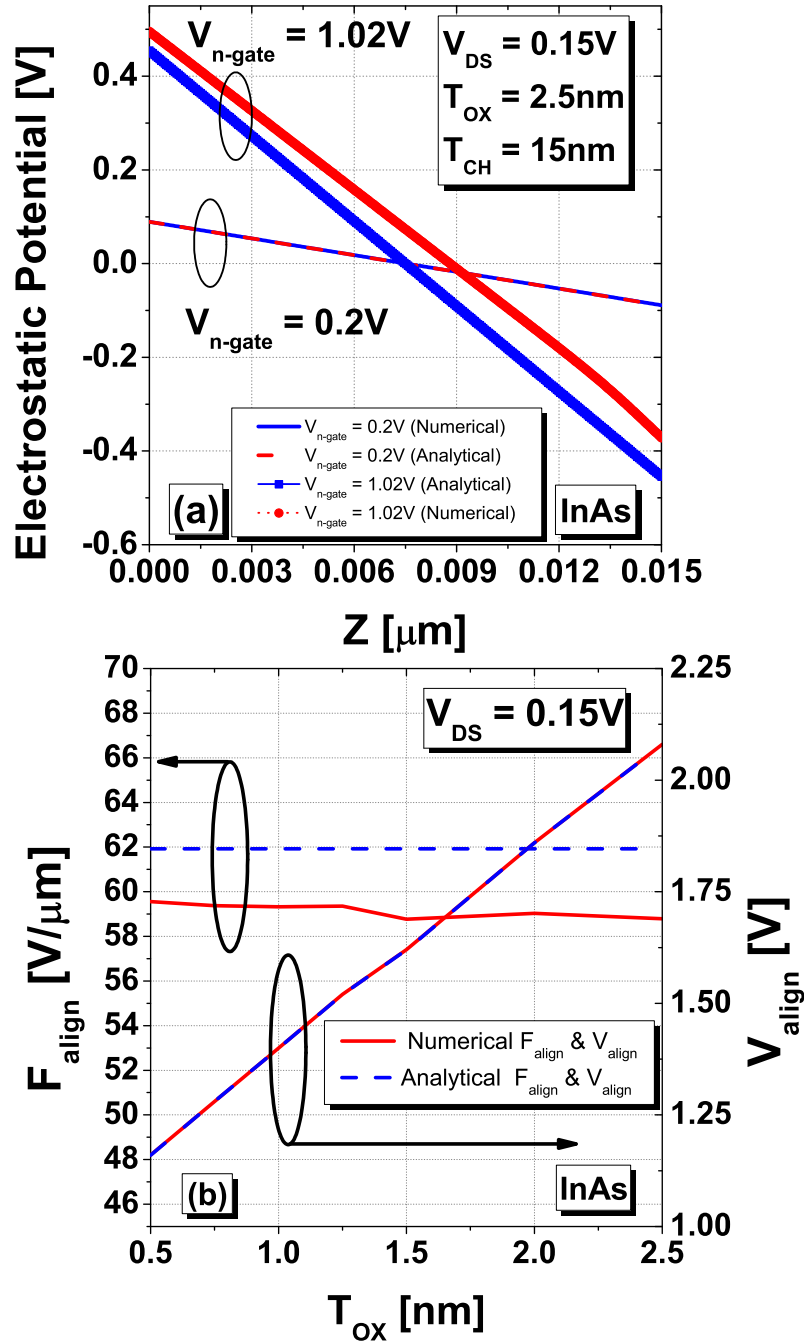
Fig. 6. (a) Potential profiles given by the numerical (blue) and analytical (red) models for high (symbols) and low (lines) applied gate voltages for the InAs EHBTFET. $z = 0$ and $z = T_{\mathrm{CH}}$ corresponds to n-gate and p-gate oxide-semiconductor interface respectively. (b) Alignment field F_{align} and alignment voltages predicted by the numerical (solid lines) and analytical (dashed lines) models.

Since the potential is (to a very good approximation) linear, the quantized energies $E_{\mathrm{e(h)}}$ and wavefunctions $\psi_{\mathrm{e(h)}}$ are given by the solutions for the triangular potential well, for which analytical expressions exist [29]. The alignment occurs when

(considering direct tunneling) $E_\text{e} = E_\text{h}$ [7], i.e. when:

$$E_\text{C}(0) - a_1 \sqrt[3]{\frac{q^2 F_\text{align}^2 \hbar^2}{2m_e^*}} = E_\text{V}(T_\text{CH}) + a_1 \sqrt[3]{\frac{q^2 F_\text{align}^2 \hbar^2}{2m_h^*}} \tag{6}$$

which can be rewritten as:

$$E_\text{G} - a_1 \sqrt[3]{\frac{q^2 F_\text{align}^2 \hbar^2}{2m_e^*}} - a_1 \sqrt[3]{\frac{q^2 F_\text{align}^2 \hbar^2}{2m_h^*}} = q F_\text{align} T_\text{CH} \tag{7}$$

where $a_1 = -2.338$ is the first zero of the Airy function given by the solution of the triangular potential well, F_align is value of the electric field parameter F at subband alignment. Eq. 7 holds for direct BTBT process, whereas a similar expression (including the phonon energy) exists for phonon-assisted tunneling. Two key insights can be inferred from Eq. 7: i) the numerical results are confirmed about the dependences of the I_ON in 2D-2D tunneling since the equation has no T_OX dependent terms, ii) for a given T_CH, the alignment always occurs at a certain magnitude of the electric field F_align, which is the solution of Eq. 7. The comparison between the numerically calculated and analytical F_align values (given in Fig. 6(b)), indicates good overall matching (maximum difference $\sim 6\%$ for the considered plot).

Now, we turn our attention to the implications of the fixed electric field at alignment on the wavefunctions. Within the triangular approximation, the analytical expressions for the electron and hole wavefunctions at subband alignment are given as [29]:

$$\psi_e(z) = D \text{Ai}\left(\left(\frac{2m_e^*}{\hbar^2}(qF_\text{align})\right)^{\frac{1}{3}}(z - z^*)\right) \tag{8}$$

$$\psi_h(z) = D \text{Ai}\left(-\left(\frac{2m_h^*}{\hbar^2}(qF_\text{align})\right)^{\frac{1}{3}}(z - z^*)\right) \tag{9}$$

where Ai is the Airy function, z^* is the classical turning point at which $E_\text{C(V)} = E_\text{e(h)}$ and D is a normalization constant. It is easily seen that the wavefunctions are fixed by F_align, since it is the only factor governed by the electrostatics. By inspecting Eq. 2, the coupling element M_dir is thus deduced to be fixed as well. The magnitude of the coupling element is given by the channel material properties and by the channel thickness only. The same holds for phonon-assisted BTBT since the wavefunction overlap remains fixed too. We note that the arguments presented above are valid when the triangular potential approximation holds, i.e. in the absence of inversion layers inside the device. In the presence of an inversion layer, detrimental effects such as pinning of the surface potential that decrease in the 'quantum efficiency' [7] and ultimately a decrease in the switching slope might occur.

Making use of the analytical model, the alignment voltage V_align can be calculated using the following formula:

$$V_\text{align} = F_\text{align}\left(T_\text{CH} + 2\frac{\epsilon_\text{CH}}{C_\text{OX}}\right) \tag{10}$$

As seen in Fig. 6(b), Eq. 10 predicts V_align excellent accuracy. On the other hand, F_align is overestimated by the analytical model compared to the numerical results because it uses parabolic approximation, whereas in the numerical model nonparabolicity corrections slightly reduce the quantization energies and therefore F_align.

The findings above signal that the optimization strategy for the EHBTFET with certain performance constraints is to determine the channel material and T_CH first according to I_ON requirements, and then, using Eq. 10, estimate the required C_OX for the desired operating voltages and switching slope requirements.

C. Performance Considerations & Impact of Channel Material

In addition to the qualitative and theoretical assessments discussed above, certain inferences can be made about the performance limits (in terms of ON current) of the EHBTFETs with the different channel materials considered here. Bearing in mind that EHBTFET is considered mainly for low power and low standby power applications [30], we set an alignment voltage limit of 2V (see Fig. 3). This constraint can be partially achieved through gate workfunction engineering i.e. the 2V obtained here with mid-gap metal work-functions can be achieved with lower applied bias, e.g. just above 1V, if n- and p-type workfunctions are used for the top and bottom gate, respectively [31].

Within this constraint, InAs seems to offer the best $I_\text{ON,max} \sim 1.75 \text{mA}/\mu\text{m}$ compared to Ge ($I_\text{ON,max} \sim 3.34 \mu\text{A}/\mu\text{m}$) and $\text{In}_{0.53}\text{Ga}_{0.47}\text{As}$ ($I_\text{ON,max} \sim 1 \mu\text{A}/\mu\text{m}$), whereas it is not even possible to obtain 2D-2D tunneling for Si and $\text{Si}_{0.5}\text{Ge}_{0.5}$. Moreover, the InAs EHBTFET can also be operated at an even lower V_align of 1V, of course with lower $I_\text{ON,max} \sim 26 \mu\text{A}/\mu\text{m}$, by using larger $T_\text{CH} \sim 19\text{nm}$. Even though the bandgaps are comparable for Ge and $\text{In}_{0.53}\text{Ga}_{0.47}\text{As}$, the obtainable ON current is drastically higher for $\text{In}_{0.53}\text{Ga}_{0.47}\text{As}$ for a given channel thickness since it is a direct gap material. However, this advantage of $\text{In}_{0.53}\text{Ga}_{0.47}\text{As}$ over Ge for the same channel thickness does not show up when we impose the alignment voltage constraint. This is due to the fact that the small effective mass of Γ electrons of $\text{In}_{0.53}\text{Ga}_{0.47}\text{As}$ inhibits going below a minimum allowed

TABLE II

COMPARISON OF CALCULATED CONDUCTANCE VALUES (S_{ON}) AND ALIGNMENT VOLTAGES (V_{align}). $T_{\text{OX,EOT}} = 0.8$nm.

	T_{CH}[nm]	Agarwal *et al.*		This work	
		S_{ON}[A/Vμm]	V_{align}[V]	S_{ON}[A/Vμm]	V_{align}[V]
Si	4.3	1×10^{-3}	5.55	5.93×10^{-9}	5.29
	5.9	1×10^{-5}	4.19	3.33×10^{-11}	4.05
Ge	9.7	1×10^{-3}	2.68	1.47×10^{-6}	2.64
	14.9	1×10^{-5}	1.83	4.5×10^{-9}	1.95
InAs	14.6	1×10^{-3}	1.45	1.23×10^{-4}	1.33
	24.2	1×10^{-5}	0.93	2.45×10^{-6}	0.95

channel thickness that is $T_{\text{CH,min}} \simeq 13.5$nm compared to $T_{\text{CH,min}} \simeq 10.5$nm for Ge. Small effective mass intensifies the quantization effects and results in a larger minimum allowed thickness for In$_{0.53}$Ga$_{0.47}$As.

Note that as well as the static figures of merit such as the ones investigated here, dynamic aspects such as the increased parasitic capacitances introduced by the double gate structure of the EHBTFET are also important for circuit operation. A quantitative assessment is not straighforward, since it is related to the circuit topology to be employed to drive the two gates of the EHBTFET and will need to be investigated in a future work.

An overall consistency with [6] is seen in the predicted alignment voltages (see Tab. II), although our simulations indicate orders of magnitude lower conductance levels ($S_{\text{ON}} = \frac{\partial I_{\text{D}}}{\partial V_{\text{DS}}}$ at first subband alignment) than in [6] for Si and Ge. This is due to the use of a direct tunneling matrix element in Agarwal *et al.* that largely differs from the phonon assisted tunneling one [16] that we found to be dominant in Si and Ge devices. Even though direct BTBT is dominant in Ge for bulk 3D-3D tunneling [8], quantization essentially suppresses the direct BTBT in the ON state of the Ge EHBTFET for all the cases considered in this study. Regarding InAs, instead, our results are only 5-10 times lower than the ones in [6] mainly due to the inclusion in our model of the effect of quantization on the matrix element (term $C_0(\theta)$ in Eq. 2)[14].

V. CONCLUSION

An extensive analysis for EHBTFETs using different channel thicknesses and materials as well as oxide thicknesses has been performed. Striking differences in geometrical parameter dependences of the I_{ON} is observed between 2D-2D tunneling (InAs, In$_{0.53}$Ga$_{0.47}$As and Ge) and 3D-3D tunneling (Si and Si$_{0.5}$Ge$_{0.5}$). For 2D-2D tunneling with a chosen channel thickness, the alignment always occurs at a certain F_{align}, fixing the overlap between the electron and hole wavefunctions. This exclusive feature of 2D-2D tunneling, along with the step-like characteristic of the 2D DOS, imposes an upper limit on the I_{ON} that can be obtained, contrary to 3D-3D tunneling. This limit depends on the channel thickness and on the material properties, whereas it is independent on electrostatic control of the channel. Among the considered materials in this work, it is seen that InAs is a prominent candidate for the realization of 2D-2D tunneling devices, since it has relatively low alignment voltages and very high ON current levels. Lower alignment voltages could be obtained by creating staggered gap heterojunctions in the channel such as InAs/GaSb. Similarly, strain can be utilized to enhance the performance of III-V based TFETs [32] and GeSn alloys can promote direct BTBT [33] compared to the pure Ge considered here and this may result in a sizable improvement of the ON current. An analytical model providing a very good approximation to the vertical potential profile of the EHBTFET is also proposed and the numerical findings are verified through this model and triangular well approximation.

REFERENCES

[1] U. E. Avci, D. H. Morris, and I. A. Young, "Tunnel Field-Effect Transistors: Prospects and Challenges," *IEEE Journal of the Electron Devices Society*, vol. 3, no. 3, pp. 88–95, 2015.

[2] D. Sarkar, X. Xie, W. Liu, W. Cao, J. Kang, Y. Gong, S. Kraemer, P. M. Ajayan, and K. Banerjee, "A subthermionic tunnel field-effect transistor with an atomically thin channel," *Nature*, vol. 526, no. 7571, pp. 91–95, 2015.

[3] A. M. Ionescu and H. Riel, "Tunnel field-effect transistors as energy-efficient electronic switches.," *Nature*, vol. 479, pp. 329–37, Nov. 2011.

[4] L. Lattanzio, L. De Michielis, and A. M. Ionescu, "Electron-hole bilayer tunnel FET for steep subthreshold swing and improved ON current," in *2011 Proceedings of the European Solid-State Device Research Conference (ESSDERC)*, pp. 259–262, IEEE, Sept. 2011.

[5] C. Alper, P. Palestri, L. Lattanzio, J. L. Padilla, and A. M. Ionescu, "Two dimensional quantum mechanical simulation of low dimensional tunneling devices," *Solid-State Electronics*, vol. 113, pp. 167–172, Nov. 2015.

[6] S. Agarwal, J. T. Teherani, J. L. Hoyt, D. A. Antoniadis, and E. Yablonovitch, "Engineering the Electron-Hole Bilayer Tunneling Field-Effect Transistor," *IEEE Transactions on Electron Devices*, vol. 61, no. 5, pp. 1599–1606, 2014.

[7] J. T. Teherani, S. Agarwal, E. Yablonovitch, J. L. Hoyt, and D. A. Antoniadis, "Impact of Quantization Energy and Gate Leakage in Bilayer Tunneling Transistors," *IEEE Electron Device Letters*, vol. 34, pp. 298–300, Feb. 2013.

[8] C. Alper, P. Palestri, J. L. Padilla, A. Gnudi, R. Grassi, E. Gnani, M. Luisier, and A. M. Ionescu, "Efficient quantum mechanical simulation of band-to-band tunneling," in *EUROSOI-ULIS 2015: 2015 Joint International EUROSOI Workshop and International Conference on Ultimate Integration on Silicon*, pp. 141–144, 2015.

[9] A. Trellakis, A. T. Galick, A. Pacelli, and U. Ravaioli, "Iteration scheme for the solution of the two-dimensional Schrodinger-Poisson equations in quantum structures," *Journal of Applied Physics*, vol. 81, no. 12, p. 7880, 1997.

[10] C. Troger, H. Kosina, and S. Selberherr, "Modeling nonparabolicity effects in silicon inversion layers," in *SISPAD '97. 1997 International Conference on Simulation of Semiconductor Processes and Devices. Technical Digest*, pp. 323–326, Ieee, 1997.

[11] A. Rahman, M. S. Lundstrom, and A. W. Ghosh, "Generalized effective-mass approach for n-type metal-oxide-semiconductor field-effect transistors on arbitrarily oriented wafers," *Journal of Applied Physics*, vol. 97, no. 5, p. 053702, 2005.

[12] C. Alper, L. Lattanzio, L. De Michielis, P. Palestri, L. Selmi, and A. M. Ionescu, "Quantum Mechanical Study of the Germanium ElectronHole Bilayer Tunnel FET," *IEEE Transactions on Electron Devices*, vol. 60, pp. 2754–2760, Sept. 2013.

[13] A. Schenk, M. Stahl, and H.-J. Wünsche, "Calculation of Interband Tunneling in Inhomogeneous Fields," *Phys. Status Solidi (b)*, vol. 154, pp. 815–826, Aug. 1989.

[14] M. Yamanishi and I. Suemune, "Comment on Polarization Dependent Momentum Matrix Elements in Quantum Well Lasers," *Japanese Journal of Applied Physics*, vol. 23, pp. L35–L36, Jan. 1984.

[15] H. Carrillo-Nuñez, A. Ziegler, M. Luisier, and A. Schenk, "Modeling direct band-to-band tunneling: From bulk to quantum-confined semiconductor devices," *Journal of Applied Physics*, vol. 117, p. 234501, June 2015.

[16] W. G. Vandenberghe, B. Soree, W. Magnus, G. Groeseneken, and M. Fischetti, "Impact of field-induced quantum confinement in tunneling field-effect devices," *Applied Physics Letters*, vol. 98, no. 14, p. 143503, 2011.

[17] S. Jin, A. T. Pham, Woosung Choi, Y. Nishizawa, Young-Tae Kim, Keun-Ho Lee, Youngkwan Park, and Eun Seung Jung, "Performance evaluation of InGaAs, Si, and Ge nFinFETs based on coupled 3D drift-diffusion/multisubband boltzmann transport equations solver," in *2014 IEEE International Electron Devices Meeting*, pp. 7.5.1–7.5.4, 2014.

[18] C. Alper, M. Visciarelli, P. Palestri, J. L. Padilla, A. Gnudi, E. Gnani, and A. M. Ionescu, "Modeling the imaginary branch in III-V tunneling devices: Effective mass vs k.p," in *2015 International Conference on Simulation of Semiconductor Processes and Devices (SISPAD)*, pp. 273–276, IEEE, Sept. 2015.

[19] Q. Zhang, S. Sutar, T. Kosel, and A. Seabaugh, "Fully-depleted Ge interband tunnel transistor: Modeling and junction formation," *Solid-State Electronics*, vol. 53, pp. 30–35, Jan. 2009.

[20] W. G. Vandenberghe and M. V. Fischetti, "Deformation potentials for band-to-band tunneling in silicon and germanium from first principles," *Applied Physics Letters*, vol. 106, no. 1, p. 013505, 2015.

[21] P. M. Solomon, "Universal tunneling behavior in technologically relevant P/N junction diodes," *Journal of Applied Physics*, vol. 95, no. 10, p. 5800, 2004.

[22] A. M. Walke, A. S. Verhulst, A. Vandooren, D. Verreck, E. Simoen, V. R. Rao, G. Groeseneken, N. Collaert, and A. V. Y. Thean, "Part I: Impact of field-induced quantum confinement on the subthreshold swing behavior of line TFETs," *IEEE Transactions on Electron Devices*, vol. 60, no. 12, pp. 4057–4064, 2013.

[23] J. L. Padilla, C. Alper, F. Gámiz, and A. M. Ionescu, "Assessment of field-induced quantum confinement in heterogate germanium electronhole bilayer tunnel field-effect transistor," *Applied Physics Letters*, vol. 105, p. 082108, Aug. 2014.

[24] C. Alper, P. Palestri, J. L. Padilla, and A. M. Ionescu, "Underlap counterdoping as an efficient means to suppress lateral leakage in the electronhole bilayer tunnel FET," *Semiconductor Science and Technology*, vol. 31, no. 4, p. 045001, 2016.

[25] A. W. Dey, B. M. Borg, B. Ganjipour, M. Ek, K. a. Dick, E. Lind, C. Thelander, and L.-E. Wernersson, "High-Current GaSb/InAs(Sb) Nanowire Tunnel Field-Effect Transistors," *IEEE Electron Device Letters*, vol. 34, pp. 211–213, Feb. 2013.

[26] H. Lu and A. Seabaugh, "Tunnel Field-Effect Transistors: State-of-the-Art," *IEEE Journal of the Electron Devices Society*, vol. 2, pp. 44–49, July 2014.

[27] K.-H. Kao, A. S. Verhulst, W. G. Vandenberghe, B. Soree, G. Groeseneken, and K. De Meyer, "Direct and Indirect Band-to-Band Tunneling in Germanium-Based TFETs," *IEEE Transactions on Electron Devices*, vol. 59, pp. 292–301, Feb. 2012.

[28] R. H. Yan, A. Ourmazd, and K. F. Lee, "Scaling the Si MOSFET: From bulk to SOI to bulk," *IEEE Transactions on Electron Devices*, vol. 39, no. 7, pp. 1704–1710, 1992.

[29] F. Stern, "Self-consistent results for n-type Si inversion layers," *Physical Review B*, vol. 5, no. 12, pp. 4891–4899, 1972.

[30] A. R. Trivedi, S. Carlo, and S. Mukhopadhyay, "Exploring tunnel-FET for ultra low power analog applications," *Proceedings of the 50th Annual Design Automation Conference*, no. V, pp. 109:1—109:6, 2013.

[31] J. L. Padilla, C. Alper, A. Godoy, F. Gamiz, and A. M. Ionescu, "Impact of Asymmetric Configurations on the Heterogate Germanium Electron-Hole Bilayer Tunnel Field-Effect Transistor Including Quantum Confinement," *IEEE Transactions on Electron Devices (Available Online)*, 2015.

[32] F. Conzatti, M. G. Pala, D. Esseni, E. Bano, and L. Selmi, "Strain-induced performance improvements in InAs nanowire tunnel FETs," *IEEE Transactions on Electron Devices*, vol. 59, no. 8, pp. 2085–2092, 2012.

[33] C. Schulte-Braucks, D. Stange, N. von den Driesch, S. Blaeser, Z. Ikonic, J. M. Hartmann, S. Mantl, and D. Buca, "Negative differential resistance in direct bandgap GeSn p-i-n structures," *Applied Physics Letters*, vol. 107, no. 4, p. 042101, 2015.